
Faculty of Science

Faculty Publications

This is a post-print version of the following article:

Microfluidic Manufacturing of Polymeric Nanoparticles: Comparing Flow Control of Multiscale Structure in Single-Phase Staggered Herringbone and Two-Phase Reactors

Zheqi Xu, Changhai Lu, Jason Riordan, David Sinton, & Matthew G. Moffitt

November 2016

The final publication is available at:

<https://doi.org/10.1021/acs.langmuir.6b03243>

Citation for this paper:

Xu, Z., Lu, C., Riordan, J., Sinton, D., & Moffitt, M. G. (2016). Microfluidic Manufacturing of Polymeric Nanoparticles: Comparing Flow Control of Multiscale Structure in Single-Phase Staggered Herringbone and Two-Phase Reactors. *Langmuir*, 32(48), 12781-12789. <https://doi.org/10.1021/acs.langmuir.6b03243>.

Microfluidic Manufacturing of Polymeric Nanoparticles: Comparing Flow Control of Multiscale Structure in Single-Phase Staggered Herringbone and Two-Phase Reactors

Zheqi Xu,[†] Changhai Lu,[†] Jason Riordon,[‡] David Sinton,[‡] and Matthew G. Moffitt*[†]

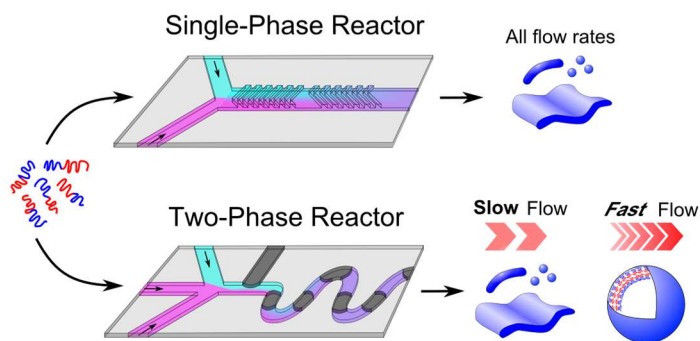
[†] *Department of Chemistry, University of Victoria, P.O. Box 3065, Victoria, BC, Canada V8W 3V6*

[‡] *Department of Mechanical and Industrial Engineering and Institute for Sustainable Energy, University of Toronto, 5 King's College Road, Toronto, ON, Canada, M5S 3G8*

Abstract

We compare microfluidic manufacturing of polycaprolactone-*block*-poly(ethylene oxide) (PCL-*b*-PEO) nanoparticles (NPs) in a single-phase staggered herringbone (SHB) mixer and in a two-phase gas-liquid segmented mixer. NPs generated from two different copolymer compositions in both reactors and at three different flow rates, along with NPs generated using a conventional bulk method, are compared with respect to morphologies, dimensions, and internal crystallinities. Our work, the first direct comparison between alternate microfluidic NP synthesis methods, shows three key findings: (i) NP morphologies and dimensions produced in the bulk are different from those produced in either microfluidic mixer, whereas NP crystallinities produced in the bulk and in the SHB mixer are similar; (ii) NP morphologies, dimensions, and crystallinities produced in the single-phase SHB and two-phase mixers at the lowest flow rate are similar; and (iii) NP morphologies, dimensions, and crystallinities change with flow rate in the two-phase mixer but not in the single-phase SHB mixer. These findings provide new insights into the relative roles of mixing and shear in the formation and flow-directed processing of polymeric NPs in microfluidics, informing future reactor designs for manufacturing NPs of low polydispersity and controlled multiscale structure and function.

Table of Content Graphic:



Introduction

In the past decade, there has been tremendous progress in the development of microfluidic systems for chemical and nanoparticle (NP) synthesis.¹⁻¹² The high-precision control of flow rates, small reagent consumption, enhanced heat transfer, and ability to incorporate several processes onto one device, make microfluidics a very convenient platform for synthesis,² and provide access to mass transfer rates not achievable in bulk systems.¹³ For drug delivery applications, these features enable fast and efficient screening of chemical and processing parameters for manufacturing polymeric or phospholipid NPs loaded with therapeutic molecules;^{5,14} as well, a variety of microfluidic approaches have been applied to control NP shape,¹⁵⁻²⁰ size,^{3,14,21-30} polydispersity,²²⁻²⁴ and internal structure,^{19,20} all germane structural parameters for achieving optimal targeted delivery.¹⁹ An inherent feature of synthesis in microfluidic channels is that low-Reynolds number conditions give rise to laminar flow of converging liquid streams, such that mixing between streams is diffusion-dominated without the advection contributions of turbulent flow.³¹ Therefore, microfluidic mixers must be specially designed to decrease diffusional path lengths and increase contact area between liquid streams in order to achieve fast mixing.¹⁴ In general, microfluidic mixers can be divided into single-phase^{22,24,28,31-37} and two-phase reactors.^{38,39}

Single-phase reactors are those in which all inlet streams contain miscible liquids, and encompass a wide variety of mixing strategies, including hydrodynamic focussing,³² dividing of liquid streams,³⁷ and the introduction of ribs or grooves within the channels.^{31,33-35} For example, the Whitesides group developed a staggered herringbone mixer (SHM) with a groove pattern on the floor of the microchannel;^{33,34} this topology generates three-dimensional twisting flow which greatly increases the rate of mixing between streams. The SHM system has been applied to the

synthesis of phospholipid NPs for drug and siRNA delivery, resulting in smaller NP size and lower polydispersities than are achievable using conventional methods.^{22,28}

Two-phase reactors are those in which mixing components enter the reactor in miscible liquid streams, while another inlet provides either an immiscible liquid (liquid-liquid reactors)³⁸ or a gas (gas-liquid reactors),³⁹ in order to develop segmented flow with regular spacing of moving interfaces (liquid-liquid or gas-liquid). In these reactors, fast mixing is provided by counter-rotating vortices within liquid aqueous droplets dispersed within an oil phase (liquid-liquid reactors)³⁸ or liquid plugs separated by gas bubbles (gas-liquid reactors).³⁹ Our group has applied gas-liquid two-phase reactors to the production of a wide range of NP systems, including micellar polymer NPs of polystyrene-*block*-poly(acrylic acid) (PS-*b*-PAA),^{15-17,40} photoactive polymer NPs,¹⁸ and drug delivery NPs of biocompatible polycaprolactone-*block*-poly(ethylene oxide) (PCL-*b*-PEO).^{19,20} For each of these systems produced in gas-liquid two-phase reactors, we have reported continuous variability of NP structure (size,^{16,29,30} morphology,^{15-20,40} internal crystallinity,^{19,20} etc.) and function (photoresponsivity,¹⁸ drug/probe loading,^{17,19,20} release rates,^{17,19,20} etc.) simply by changing the total flow rate.

Due to the lack of direct comparison studies, the coupled effects of fast mixing and shear on the multiscale structure of polymeric NPs synthesized within single-phase SHB and two-phase microfluidic reactors remains poorly understood. Our current understanding is that the observed flow dependences of structure and function for NP synthesis in two-phase gas-liquid reactors are due to high-shear effects,^{15,17-19,29,30} rather than the effects of fast mixing which are common to both single-phase SHB and two-phase microfluidic mixers. Computational fluid dynamics calculations have shown highly localized high-shear regions in the corners of the liquid plugs of two-phase gas-liquid reactors with maximum shear rates ($\sim 10^5$ - 10^6 s⁻¹) that

increase linearly with total flow rate.^{29,30} It has been proposed that these high shear rates give rise to significant particle processing as particles circulate through the hot spots, leading to flow-dependent structural parameters including sizes and morphologies influenced by shear-induced particle coalescence or breakup^{15,30} and internal structure governed by shear-induced polymer crystallization.¹⁹ In contrast, much lower maximum shear rates have been reported at the walls of single-phase SHB mixers ($\sim 10^2$ - 10^3 s⁻¹);³⁶ based on Peclet and capillary numbers achievable under these shear conditions, significant processing of NPs *via* shear effects is not expected in these reactors. This analysis is supported by a recent study on the effects of total flow rates and flow rate ratios on the sizes, polydispersities, and transfection efficiencies of liposomes manufactured in SHB mixers, which showed that while flow rate ratio (and hence on-chip chemical composition) significantly affected NP characteristics, total flow rate (and hence maximum shear rate) did not.²⁴ In another study, the sizes of polydiacetylene NPs produced in a SHB reactor were found to decrease with total flow rate, but only in a regime of very low flow rates (~ 20 - 60 $\mu\text{L} / \text{min}$) where size variation was attributed to differences in mixing times rather than shear effects.²¹ To our knowledge, a study directly comparing microfluidic flow rate dependencies on the structural features of NPs produced in a single-phase SHB mixer and a two-phase gas-liquid mixer has not been previously carried out.

In this study, we compare these two common reactor designs with respect to NP formation from the same two PCL-*b*-PEO copolymers (identical PEO block lengths and two different PCL block lengths), both under identical chemical conditions and for an identical set of flow rates. NP morphologies and core dimensions are characterized by transmission electron microscopy (TEM), and internal PCL crystallinities are characterized by powder x-ray diffraction (XRD). For both copolymers, we find flow dependencies on the morphology and multiscale structure

(core dimensions and internal crystallinities) in the high-shear, two-phase mixer that are not found in the low-shear, single-phase SHB mixer. Both reactors produce NP morphologies and dimensions that are different from NPs formed from equivalent copolymers using bulk mixing. These results indicate that fast mixing in microfluidic mixers produces polymeric NPs that are unique from those formed by conventional bulk methods. Our results also underline the critical role of the high-shear environment in two-phase microfluidic mixers for the flow-dependent particle processing of polymeric NPs in these reactors. Finally, this work allows us to decouple for the first time mixing and shear effects in two-phase microfluidic mixers.

Experimental

Materials. Stannous octonate (95%), PEG methyl ether (MePEG-OH, MW~5000) and ϵ -caprolactone (97%) were all purchased from Sigma-Aldrich and used for the synthesis of the PCL-5k copolymer. Toluene (Caledon, 99.5%) and dimethylformamide (DMF, Caledon, 99.8%) were used as received without further purification. PCL₁₀₅-*b*-PEO₁₁₄ (PCL-12k) was purchased from Advanced Polymer Materials Inc; numbers in subscripts describe number-average degrees of polymerization of the respective blocks.

Synthesis of PCL₄₄-*b*-PEO₁₁₄ Copolymer (PCL-5k). The copolymer was synthesized *via* ring opening polymerization of ϵ -caprolactone (ϵ -CL) in the presence of MePEG-OH as the macroinitiator and stannous octonate (Sn(Oct)₂) as the catalyst.⁴¹ The polymerization was carried out under nitrogen atmosphere in a flame-dried round-bottom flask. In brief, following azeotropic distillation in toluene, 5 g of MePEG-OH (1 mmol) was dissolved in a 75 ml volume of dried toluene and ϵ -CL (5 g, 43.85 mmol) and Sn(Oct)₂ were added to the reaction vessel. The

polymerization was carried out at 110 °C for 24 hrs with continuous stirring. The copolymer was isolated by precipitation in cold ether and dried under vacuum, followed by characterization with ^1H NMR and GPC. Characteristics of the copolymers are tabulated in Table 1.

Critical Water Content (cwc) Determination. Critical water contents were determined for both copolymers in DMF at an initial concentration of 0.33 wt %, *via* dropwise water addition monitored by static light scattering intensity measurements. Light scattering experiments were performed on a Brookhaven Instruments photocorrelation spectrometer equipped with a BI-200SM goniometer, a BI-9000AT digital autocorrelator, and a Melles Griot He-Ne Laser (632.8 nm) with a maximum power output of 75 mW, at a scattering angle of 90° and a temperature of 23 °C. For both copolymers, a 0.66 wt % solution in DMF was prepared and allowed to equilibrate overnight. This stock solution was then filtered through $2 \times 0.45 \mu\text{m}$ teflon syringe filters (VWR) in series and then diluted to a final concentration of 0.33 wt % using filtered DMF ($2 \times 0.20 \mu\text{m}$ teflon syringe filter, National Scientific). To initiate NP formation, filtered deionized water ($2 \times 0.20 \mu\text{m}$ Nylon syringe filters, National Scientific) was added in successive 0.03-0.06 g quantities to this solution. After each addition of water, the solution was vortexed to help mixing and then equilibrated for 15 min before the scattered light intensity was measured. From the resulting plots of scattered light intensity vs. water concentration, cwc values were determined by extrapolation of the steep increase in intensity to the baseline. A sample curve for the PCL-5k copolymer is shown in Figure S1; cwc values for both copolymers are tabulated in Table 1 and were used as reference values for selecting water contents for bulk and microfluidic NP preparations. Errors on cwc values are standard deviations from triplicate cwc determinations.

Table 1. Copolymer Characteristics and Critical Water Contents.

Copolymer	m^a	n^a	PDI	cwc ^b / wt %
PCL-5k	44	114	2.0 ^c	7.1 ± 0.2
PCL-12k	105	114	1.1	5.5 ± 0.1

a) m and n are the number-average degrees of polymerization of the PCL and PEO blocks, respectively.

b) Critical water contents (cwc) were determined for the respective copolymer solutions in DMF at an initial polymer concentration of 0.33 wt %.

c) Calculated from $PDI = M_w/M_n$ with M_n determined from NMR and M_w from GPC.

Bulk Preparation of PCL-*b*-PEO NPs. As a control experiment for comparison with NP formation in single-phase SHB and two-phase microfluidic reactors, NPs of both block copolymer were formed by the conventional method of dropwise water addition. For these experiments, deionized water was added dropwise to 3 g of 0.33 wt % copolymer solution in DMF at a rate of 20 μ L every 10 s up to a target water content of cwc + 10 wt % with moderate stirring.

NanoAssemblr™ Benchtop Microfluidic Mixer (Single-Phase SHB Reactor). A commercial SHM-based microreactor for benchtop production of lipid and polymer-based drug delivery NPs, the NanoAssemblr™, is currently available through the Vancouver-based company Precision Nanosystems Inc. The NanoAssemblr™ microfluidic mixer applied here (Figure 1A) is based on the staggered herringbone (SHB) design, and was obtained on loan from Precision Nanosystems Inc. The benchtop instrument is a syringe pump controlled by a laptop; the microfluidic reactor is fabricated in cyclic olefin copolymer (COC) with channels 79 μ m in depth and 200 μ m in width. The SHB grooves in the mixing region following the Y-junction are

raised from the bottom of the mixing channel by 31 μm with feature widths of 50 μm . The length of channel is 25 mm from each inlet to the Y-junction, and 27 mm from the Y-junction to the outlet.

Preparation of PCL-*b*-PEO NPs on NanoAssemble™ (Single-Phase SHB) Microfluidic Mixer. For preparation of NPs on the NanoAssemble™ microfluidic mixer, the following liquid streams were combined within the reactor: (1) 0.66 wt % PEO-*b*-PCL (PCL-5k or PCL-12k) solutions in DMF, (2) water/DMF mixtures of either 34.2 or 31.0 wt % water for the PCL-5k and PCL-12k copolymers, respectively. The flow rates of both streams were the same, yielding steady-state on-chip concentrations of 0.33 wt % copolymer and either 17.1 or 15.5 wt % water, corresponding to 10.0 wt % above the cwc for PCL-5k and PCL-12k, respectively. Experiments were conducted at the following variable total flow rate: 20, 60 and 100 $\mu\text{L}/\text{min}$. For each condition, the outlet stream of NPs in DMF/water was collected into an empty vial for characterization.

Gas-Liquid Segmented Microfluidic Mixer (Two-Phase Reactor). The gas-liquid segmented microfluidic mixer (Figure 1B) is identical to the one employed in a recent publication, and the fabrication steps were the same as those described in that paper.¹⁸ The poly(dimethylsiloxane) reactor has a set channel depth of 150 μm and consists of a sinusoidal mixing channel 100 μm wide and a sinusoidal processing channel 200 μm wide. The length of the mixing channel is 161 mm while the length of the processing channel is 718 mm.

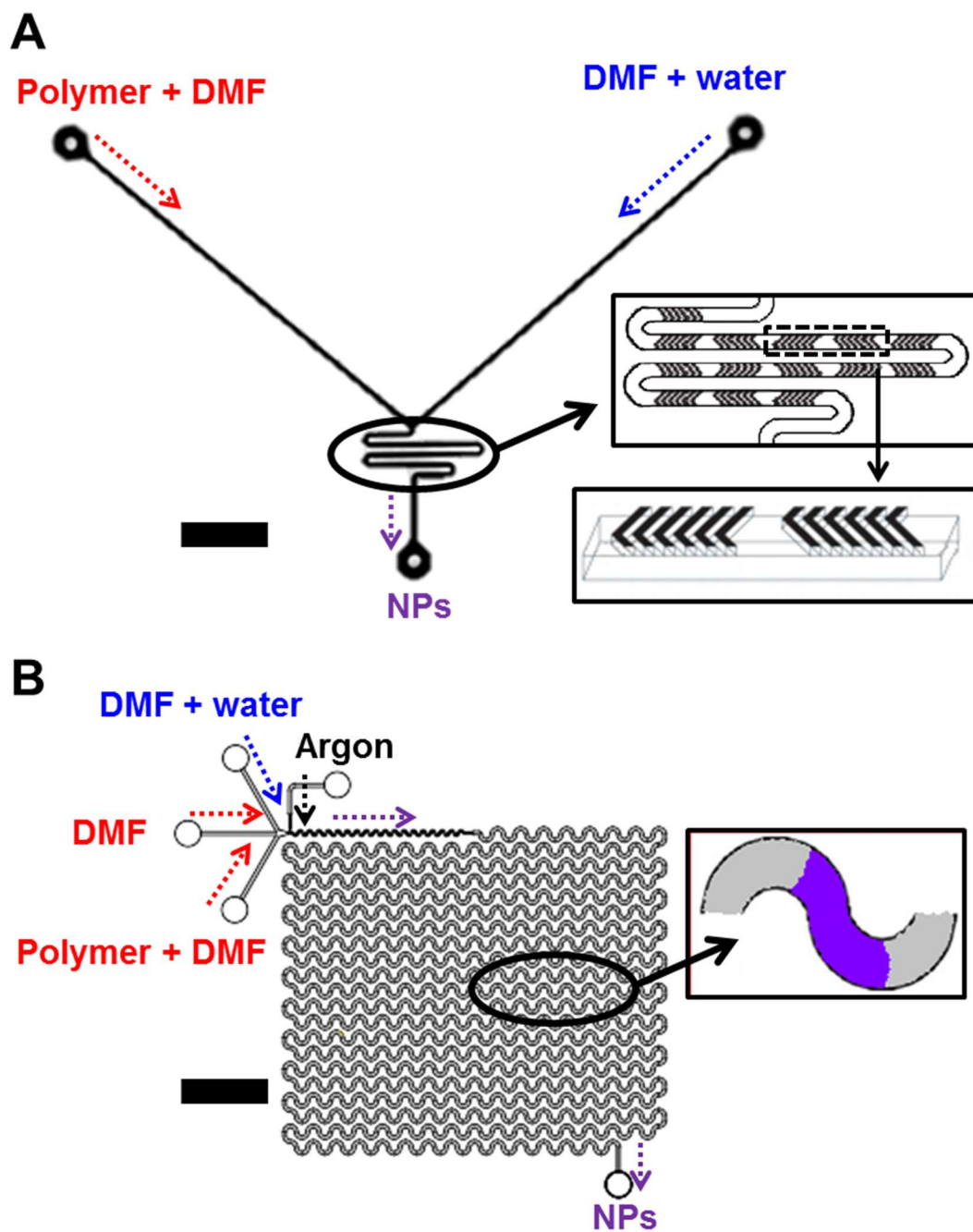


Figure 1. Schematic of single-phase SHB (A) and two-phase (B) microfluidic reactors. Scale bars are 0.5 cm.

Flow Delivery and Control on Gas-Liquid Segmented Microfluidic Mixer (Two-Phase Reactor). Pressure-driven flow of liquids to the reactor inlet was provided using 1 mL gastight syringes (Hamilton, Reno, NV) mounted on syringe pumps (Harvard Apparatus, Holliston, MA). The microfluidic chip was connected to the liquid syringes *via* 1/16th-inch (OD) Teflon tubing (Scientific Products and Equipment, ON). Gas flow was introduced to the chip *via* an Ar tank regulator and a downstream regulator (Johnston Controls) for fine adjustments. The chip was connected to the downstream regulator through a 1/16th-inch (OD) / 100- μ m (ID) Teflon tube (Upchurch Scientific, Oak Harbor, WA). The liquid flow rate (Q_{liq}) was programmed *via* the syringe pumps and the gas flow rate (Q_{gas}) was fine-tuned *via* the downstream pressure regulator in order to set the nominal total flow rates (Q_{tot}) of 20, 60 and 100 μ L/min. For all experiments, the relative gas-to-liquid flow ratio, $Q_{\text{gas}}/Q_{\text{liq}} \sim 1$.

Visualization of the gas bubbles and liquid plugs within the microfluidic reactor was achieved using an upright optical microscope (Omax) with a 10 \times objective lens. Images were captured using a 2.07 megapixel PupilCam camera (Ken-A-Vision). Actual flow parameters (within \sim 3-10 % of nominal values) pertaining to each experiment on the two-phase reactor are listed in Table S1.

Preparation of PCL-*b*-PEO NPs on Gas-Liquid Segmented Microfluidic Mixer (Two-Phase Reactor). For preparation of NPs on the gas-liquid segmented microfluidic mixer, the following three liquid streams were combined within the reactor: (1) 1.0 wt % PEO-*b*-PCL (PCL-5k or PCL-12k) solutions in DMF, (2) pure DMF, and (3) water/DMF mixtures of either 51.3 or 46.5 wt % water for the PCL-5k and PCL-12k copolymers, respectively. The flow rates of the three streams were the same, yielding steady-state on-chip concentrations of 0.33 wt % copolymer and either 17.1 or 15.5 wt % water, corresponding to 10.0 wt % above the cwc for

PCL-5k and PCL-12k respectively. Experiments were conducted at the following variable total flow rate: 20, 60 and 100 $\mu\text{L}/\text{min}$. The flow rate ratio between the three liquid inlet streams was 1:1:1, and constant for all multiphase reactor experiments. For each condition, the outlet stream of NPs in DMF/water was collected into an empty vial for characterization.

Table 2. Characteristics of Single-Phase SHB and Two-Phase Reactors

Reactor type	Flow rate ($\mu\text{L}/\text{min}$)	Mixing time (s)	Residence time (s)	Shear rate ^a (s^{-1})
Single-phase SBH	20	0.5	1	2×10^3
	60	0.2	0.5	5×10^3
	100	0.1	0.3	8×10^3
Two-phase	20	< 1	70	8×10^4
	60	< 1	20	3×10^5
	100	< 1	10	4×10^5

a) Values are average shear rates at the wall over the perimeter of the rectangular channel cross-section in the case of the single-phase SHB reactor (based on ref. 46), and maximum shear rates in the “hot spots” in the case of the two-phase reactor (based on ref. 29).

Comparison of Single-Phase (SHB) and Two-Phase Reactors. The maximum shear rates within the two-phase reactor are consistently higher (by between 1 and 2 orders of magnitude) than the perimeter-averaged shear rates at the wall for the single-phase SHB reactor, at all tested flow rates (Table 2). Calculations are based on literature empirical data for a DMF/water mixture with a DMF mole fraction of 0.6, close to the DMF mole fractions of both 17.1 wt % and 15.5 wt % water mixtures (0.54 and 0.57, respectively), measured at 25°C.⁴² Single-phase SHB mixing times (to achieve a coefficient of variation $\text{CV} < 0.1$) were estimated

based on an analytical model for a similar herringbone system presented elsewhere,⁴³ and using Péclet numbers based on the diffusion coefficient of the DMF/water mixture.^{43,44} Mixing time is inversely proportional to Reynolds number at all tested flow rates, as demonstrated elsewhere for a similar single-phase herringbone mixer.⁴³ Notably, the tested flow rates are well below the high-vorticity/low transverse flow regime, where a reduction in herringbone mixing effectiveness is expected. Final times were adjusted to compensate for the reduced cross-section of our system compared to the model. Whereas the staggered herringbone mixer's angled groove design generates strong transverse flow for rapid convective mixing,⁴⁵ the shear rate at the wall is not expected to be significantly affected by the presence of grooves, and thus calculations were based on a simplified geometry: a straight channel of rectangular cross-section.⁴⁶ Mixing rates and shear rates for the two-phase reactor were estimated based on earlier work using similar fluids and geometry and assuming a linear relationship between shear rate and flow velocity.²⁹ In the two-phase reactor, mixing is accomplished through counter-rotating vortices within flowing plugs of liquid, separated by a gas phase. The flow of bubbles force the liquid next to the walls to rapidly circulate, and create regional hot spots of elevated shear.²⁹ Residence times for both reactors are estimated based on the total fluidic volume for each reactor.

Transmission Electron Microscopy. Negatively-stained samples for TEM imaging were prepared by depositing a drop of NP dispersion on a carbon-coated 300-mesh copper TEM grid followed by a drop of 1 wt % uranyl acetate aqueous solution as a negative staining agent. Excess liquid was immediately removed using lens paper, followed by drying of the remaining liquid under ambient conditions. For unstained TEM samples, a drop of dispersion was deposited on the grid and then vitrified by flash freezing in liquid ethane followed by freeze-drying under vacuum. Imaging was performed on a JEOL JEM-1400 transmission electron microscope,

operating at an accelerating voltage of 80 kV and equipped with a Gatan Orius SC1000 CCD camera.

Averaging and statistical analysis of dimensions from TEM images were conducted using Image J software. Mean dimensions for each condition were determined from a total of ~15 images and measurement of ~400 NPs for spheres and ~150 NPs for cylinders or vesicles. Identified morphologies and mean dimensions for each NP sample are reported in Table 3. The main source of error in TEM particle sizing is spatial heterogeneity due to the non-statistical distribution of particles across the TEM grid during drying. Therefore, errors on mean dimensions reported in Table 3 represent standard deviations of mean values determined from three different regions of the grid. The resulting relative errors are <10 % in most cases, suggesting that reported mean values from TEM analysis are reliable population averages.

X-Ray Diffraction. For XRD sample preparation, solvent was removed from NP dispersions in DMF/water by rotary evaporation at 25 °C until solid films were obtained. The resulting films were then scraped as a powder onto the XRD specimen holder.

X-ray diffraction measurements were performed on a Rigaku Miniflex diffractometer with a Cr source (KR radiation, $\lambda = 2.2890 \text{ \AA}$) operating at 30 kV and 15 mA with a resolution of 0.05° (2θ) and a scan speed of $1^\circ/\text{min}$. X-ray diffraction profiles were collected for 2θ ranging from 10 - 50° .

Peak deconvolution was performed using OriginPro 2015. Two characteristic reflections for both crystalline PCL and crystalline PEO were identified and used to fix the positions of four Lorentzian peak contributions to the fit; another small Lorentzian peak contribution was used to account for a small shoulder on the more intense PCL peak in order to obtain a good fit. Thus, XRD data were fit to a sum of 6 Lorentzian functions: 3 peaks assigned to crystalline PCL ($2\theta =$

32.5, 32.7, and 35.7), 2 peaks assigned to crystalline PEO ($2\theta = 29.2$ and 35.2), and 1 peak (no fixed position) assigned to incoherent scattering from amorphous copolymer (amorphous halo). Areal peak contributions from the three components (crystalline PCL, crystalline PEO, and amorphous copolymer) were then determined by integration and percentages of crystalline PCL and PEO were calculated using:

$$\% \text{ Crystalline PCL} = A_{\text{PCL}}/A_{\text{total}} \quad (1)$$

Reported % *Crystalline* PCL values from XRD are averages determined from triplicate NP preparations under the specified conditions.

Results and Discussion

Effect of PCL Block Length on Morphologies and Core Dimensions of NPs Produced in the Bulk. In order to obtain baseline information for studying the effects of reactor design and flow rate on block copolymer self-assembly, we first determined the colloidal behaviour of the two block copolymers PCL-5k and PCL-12k when water was added using the conventional method of bulk addition. Figure 2 shows TEM images of PCL-5k and PCL-12k NPs formed in the bulk by dropwise water addition to $\text{cwc} + 10 \text{ wt } \%$. Mean core dimensions of the various morphologies from TEM size analysis are reported in Table 3. PCL-5k formed cylinders with mean widths of 32 nm along with small ~ 10 nm spheres (Figure 2A). On the other hand, PCL-12k formed pure spheres with a mean diameter of 26 nm (Figure 2B).

In the PCL-*b*-PEO copolymers used here, we see a transition from a mix of high-curvature and low-curvature morphologies (spheres and cylinders, respectively) to high-curvature morphologies (spheres) as the PCL block length increases (Figure 2). This result contrasts the behaviour of block copolymer colloids with amorphous core-forming blocks such

as PS-*b*-PAA, in which longer hydrophobic block lengths generally give rise to morphologies with less internal curvature; for example, the transition from spheres to cylinders as the PS block length increases has been reported by Eisenberg.^{47,48} However, the current trend is consistent with known effects of PCL crystallization on PCL-*b*-PEO micelle morphologies, by considering kinetic effects as water is slowly added to a crystallizable hydrophobic block. For example, in previous work on PCL-*b*-PEO self-assembly, it has been shown that spheres formed initially by dropwise water addition slowly transformed into rods over a few days under ambient conditions driven by PCL crystallization.⁴⁹ Thus, we expect that as water is added dropwise, spheres will form initially above the critical water content for both copolymers, with a thermodynamic driving force to form cylinders spurred by increasing water content and driven by PCL crystallization. PCL-5k is considerably more dynamic than PCL-12k, since its shorter PCL block forms fewer rigid PCL crystallites in the early stages of micelle formation. Therefore, PCL chains in the PCL-5k NPs (Figure 2A) are sufficiently mobile to respond to the continued increase in water content, thus rearranging on the time scale of dropwise water addition to form more crystalline cylinders. The coexisting population of small spherical micelles is explained by the longer PCL block lengths in the distribution of PCL-5k chains showing a stronger driving force to crystallize, leaving behind the shorter blocks lengths to form small ~10-nm spheres; crystallization within the cylinders eventually “locks out” the shorter PCL blocks, preventing formation of a single equilibrium morphology. In contrast, the longer PCL blocks in PCL-12k will crystallize more extensively in the early stages of micelle formation, resulting in rigid, kinetically-trapped spheres that cannot undergo further rearrangements into cylinders (Figure 2B). Thus, the comparison of kinetic structures from the bulk micellization of these two

copolymers highlights the strong effect of water addition rates on the observed morphologies of micellized PCL-*b*-PEO.

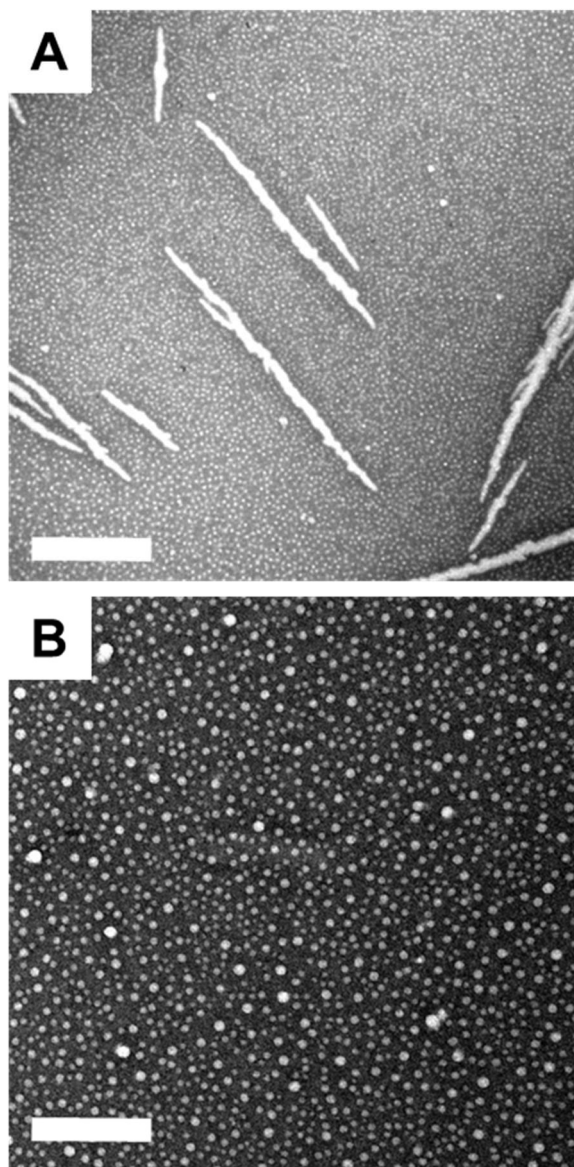


Figure 2. TEM images showing the effect of PCL block length on NP morphologies of bulk-prepared PCL-5k showing both spheres and cylinders (A), and PCL-12k showing only spheres (B). Scale bars are 400 nm.

Table 3. Morphologies^a and Mean Dimensions^{b,c} for PCL-*b*-PEO NPs Prepared in Single-Phase SHB and Two-Phase Microfluidic Reactors at Various Flow Rates.

Copolymer, Reactor	Bulk	20 $\mu\text{L}/\text{min}$	60 $\mu\text{L}/\text{min}$	100 $\mu\text{L}/\text{min}$
PCL-5k:				
Single-phase SHB	SS (9 ± 1 nm)	C (15 ± 1 nm)	C (17 ± 2 nm)	C (18 ± 1 nm)
	C (32 ± 3 nm)	L	L	L
Two-phase		C (17 ± 1 nm)	C (23 ± 2 nm)	SS (8 ± 1 nm)
		L	L	S (38 ± 2 nm)
				C (21 ± 2 nm)
				L
PCL-12k:				
Single-phase SHB		S (40 ± 2 nm)	S (40 ± 5 nm)	S (39 ± 2 nm)
		C (24 ± 2 nm)	C (26 ± 5 nm)	C (26 ± 2 nm)
	S (26 ± 1 nm)	L	L	L
Two-phase		S (41 ± 7 nm)	V (7 ± 2 nm)	
		C (21 ± 3 nm)	S? (--)	S (32 ± 1 nm)
		L		

a) Morphologies are indicated as SS (small spheres), S (spheres), C (cylinders or rods), V (vesicles) and L (lamellae).

b) Numbers refer to sphere diameters, cylinder widths or vesicle wall thickness.

c) Errors on mean dimensions represent standard deviations of mean values determined from three different regions of the grid.

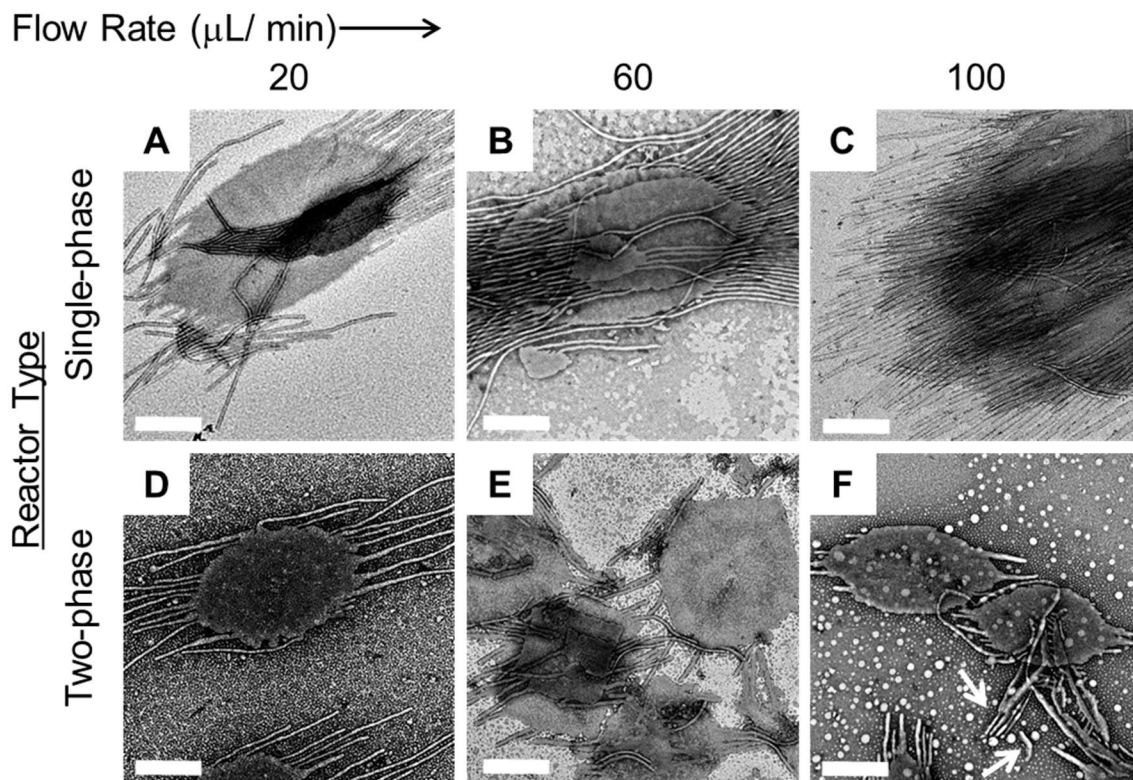


Figure 3. TEM images comparing effect of flow rate on NP morphologies of PCL-5k using single-phase SHB and two-phase microfluidic reactors. Scale bars are 400 nm. White arrows in F) show individual cylinders.

Effect of Flow Rate on Morphologies and Core Dimensions of NPs Produced in Single-Phase SHB and Two-Phase Reactors. Figure 3 compares NP morphologies of PCL-5k formed using single-phase SHB (Figure 3, A-C) and two-phase (Figure 3, D-F) microfluidic reactors at the same three total flow rates (Q_{tot}): 20, 60, and 100 $\mu\text{L} / \text{min}$. Similarly, Figure 4 compares NP morphologies of PCL-12k formed using single-phase SHB (Figure 4, A-C) and two-phase (Figure 4, D-F) microfluidic reactors at $Q_{\text{tot}} = 20, 60, \text{ and } 100 \mu\text{L} / \text{min}$. Corresponding mean core dimensions of the various morphologies are reported in Table 3.

For the PCL-5k copolymer, NPs formed in the single-phase SHB reactor (Figure 3, A-C) showed similar morphologies of lamellae with cylindrical tails at all three flow rates. Mean

dimensions in Table 3 indicate that the widths of the cylinders (~ 17 nm) formed at the three flow rates were also the same within experimental error. In contrast, NPs formed from the same copolymer in the two-phase reactor (Figure 3, D-F) showed dependence of either morphologies or core dimensions on the total flow rate. Interestingly, at $Q_{\text{tot}} = 20$ $\mu\text{L} / \text{min}$ (Figure 3D) the observed lamellae with cylindrical tails of mean width = 17 nm were identical to the morphologies and dimensions of NPs formed in the single-phase SHB reactor. Although an increase in the flow rate to $Q_{\text{tot}} = 60$ $\mu\text{L} / \text{min}$ (Figure 3E) did not change the observed mix of morphologies (lamellae with cylindrical tails), the cylinders were found to be significantly wider (23 nm) than those formed at $Q_{\text{tot}} = 20$ $\mu\text{L} / \text{min}$. Finally, at the highest flow rate of $Q_{\text{tot}} = 100$ $\mu\text{L} / \text{min}$ (Figure 3F), the mix of morphologies changed significantly; along with lamellae with cylindrical tails, individual, detached cylinders were found (Figure 3F, white arrows), with the combined mean width of cylinders (21 nm) being similar to the $Q_{\text{tot}} = 60$ $\mu\text{L} / \text{min}$ case. In addition, two new populations of small (8 nm) and larger (38 nm) spheres were identified at the highest flow rate ($Q_{\text{tot}} = 100$ $\mu\text{L} / \text{min}$, Figure 3F).

As for the PCL-5k copolymer, NPs formed from the PCL-12k copolymer in the single-phase SHB reactor (Figure 4, A-C) showed similar morphologies and core dimensions (Table 3) at all three flow rates. For the longer PCL block, the single-phase SHB reactor generated a mix of spheres (mean diameter = 40 nm), cylinders (mean width = 25 nm) and lamellae at all three flow rates, with the mean core dimensions of spheres and cylinders being the same at the different flow rates within experimental error (Table 3). Also similar to PCL-5k, NPs of PCL-12k formed in the two phase-reactor at the lowest flow rate ($Q_{\text{tot}} = 20$ $\mu\text{L} / \text{min}$, Figure 4D) showed morphologies and dimensions similar to those formed in the single-phase SHB reactor, with a mix of spheres (mean diameter = 41 nm), cylinders (mean width = 21 nm) and lamellae

generated in that case. However, increasing the flow rate in the two-phase reactor resulted in marked morphology changes. An increase in the flow rate to $Q_{\text{tot}} = 60 \mu\text{L} / \text{min}$ (Figure 4E) resulted in the formation of vesicles (wall thickness = 7 nm); vesicular walls and lumens were seen from the unstained images (Figure 4E, inset), confirming the existence of vesicles. Since spheres are not easily identified in unstained images, we cannot say conclusively whether spheres are also present in Figure 4E, although the combination of larger and smaller spherical NPs observed in the stained image suggests that both morphologies are probably present. When the flow rate was further increased to 100 $\mu\text{L}/\text{min}$ (Figure 4F), pure spheres (mean diameter = 32 nm) appeared; unstained images did not reveal vesicles at the highest flow rate. This non-monotonic trend from spheres, cylinders and lamellae, to vesicles, then to pure spheres, with increasing flow rate suggests a complex interplay of competing flow-dependent effects, including particle coalescence, breakup, and internal crystallization, as we have previously reported.^{19,20}

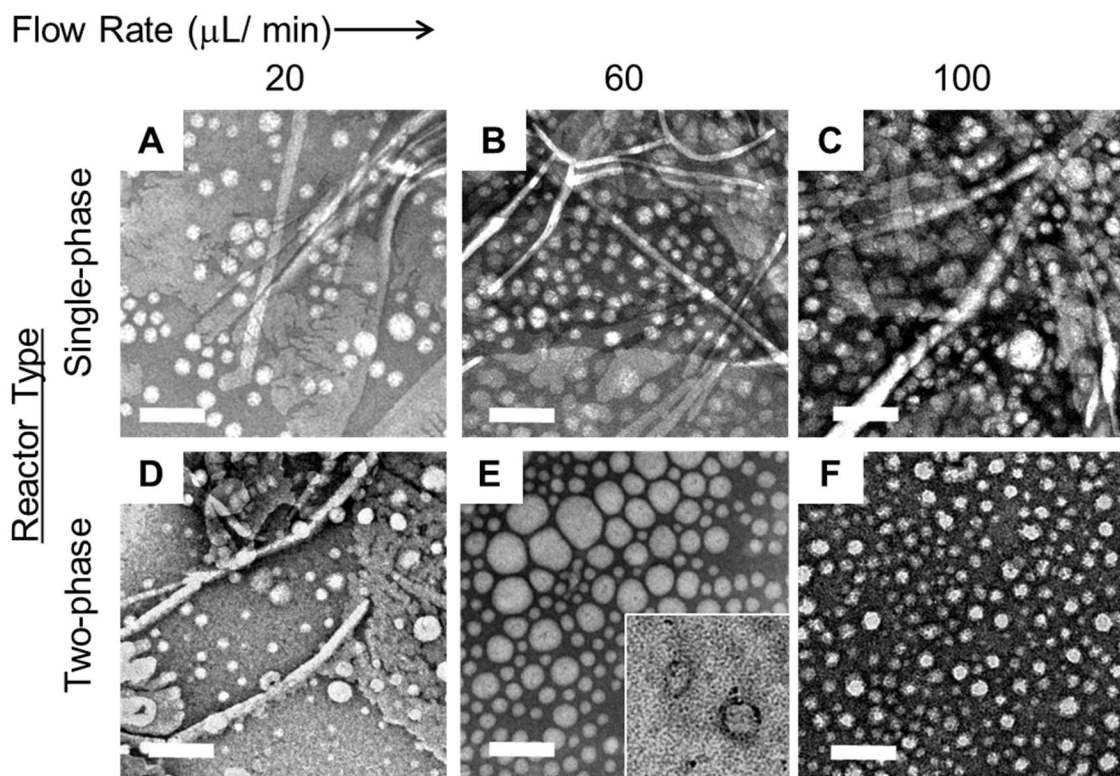


Figure 4. TEM images comparing effect of flow rate on NP morphologies of PCL-12k using single-phase SHB and two-phase microfluidic reactors. Unstained image of vesicles are shown in inset to E). Scale bars are 200 nm; scale bar in E) applies to both main image and inset.

We note three general observations common to both the PCL-5k and PCL-12k copolymers; each observation suggests a specific feature of each self-assembly environment explored here (bulk, single-phase SHB mixer, two-phase mixer). 1. *NPs formed in the bulk are different from NPs formed in either reactor (at all flow rates tested).* This finding is attributed to *slow mixing in the bulk*, compared to the fast mixing common to both microfluidic mixing strategies. As discussed in the previous section, dropwise water addition will lead to kinetic structures determined by a combination of crystallization rates and chain dynamics as the water content is gradually increased above the cwc. 2. *NPs formed in the single-phase SHB and two-phase reactors at the lowest flow rate are the same.* This finding is attributed to *similarly fast mixing*

in both microfluidic reactors, with water reaching its steady-state concentration of $c_{wc} + 10$ wt % instantaneously compared to the time scale of self-assembly in both mixers. This similarity between formation within both reactors also suggests that the condition of instantaneous mixing is achieved in both reactors even at the lowest flow rate. Finally, 3. *NP morphologies and dimensions change with increasing flow rate in the two-phase reactor but not in the single-phase SHB reactor*. This finding is attributed to *flow-dependent shear processing in the two-phase reactor* that is not present in the single-phase SHB reactor.

The comparison of single-phase SHB and two-phase reactor NPs described above provides an extremely useful handle on decoupling mixing and shear effects within two-phase mixers, as follows. The nearly identical NPs formed in the single-phase SHB reactor at all flow rates (e.g. mix of spheres, cylinders and lamellae for PCL-12k, Figure 4, A-C) reflect fast mixing in the absence of shear effects (shear processing is not expected within this type of mixer due to a combination of low shear rates and short residence times). Therefore, we infer that the same NPs will also form initially within the two-phase reactor, immediately upon fast mixing but before shear processing has taken place, irrespective of the flow rate. Then, at sufficiently high flow rates, the combination of high shear rates and long residence times within the two-phase reactor will activate various mechanisms of shear processing on initially-formed NPs (e.g. shear-induced particle breakup/coalescence), leading to the flow-dependent morphologies and dimensions of the final collected and characterized NPs (e.g. for PCL-12k, mix of vesicles and spheres at $Q_{tot} = 60 \mu\text{L} / \text{min}$, Figure 4E; and pure spheres at $Q_{tot} = 100 \mu\text{L} / \text{min}$, Figure 4F). Below a critical flow rate, the shear rate within the “hot spots” of the two-phase reactor will not be sufficiently high to activate shear processing; in these cases the initially-formed NPs are the same as those collected from the reactor (e.g. for PCL-12, mix of spheres, cylinders and lamellae at $Q_{tot} = 20$

$\mu\text{L} / \text{min}$, Figure 4D). We note that the critical flow rate below which fast mixing but not shear effects will be operative within the two-phase reactor should depend on the specific copolymer and chemical conditions; however, this parameter could always be determined by applying a comparison of single-phase SHB and two-phase reactor morphologies and dimensions at various flow rates, as described above.

Effect of Flow Rate on Core Crystallinities of NPs Produced in Single-phase SHB and Two-Phase Reactors. The effect of flow rate on the core crystallinity of NPs prepared from semicrystalline block copolymers in two-phase gas-liquid microfluidic reactors has been previously reported by our group.^{19,20} Similarly to the NP morphologies and core dimensions described above, the flow-dependent PCL crystallinity has been attributed to shear effects in the two-phase reactor.^{19,20} To provide evidence for shear-induced crystallization and also to decouple mixing and shear effects in the two-phase reactor, we now compare the PCL crystallinities of NPs prepared in single-phase SHB and two-phase reactors at four different flow rates: $Q_{\text{tot}} = 0$, 20, 60, and 100 $\mu\text{L} / \text{min}$; for both copolymers, the corresponding PCL crystallinities of the bulk-prepared NPs are used to represent the $Q_{\text{tot}} = 0$ cases. We define PCL crystallinity as the weight percentage of crystallized PCL relative to the total weight of copolymer; since the weight fractions of PCL in the PCL-5k and PCL-12k copolymers is 0.5 and 0.7, the maximum possible PCL crystallinities in these copolymers are 50% and 70%, respectively. For two copolymers (PCL-5k and PCL-12k), two reactors (single-phase SHB and two-phase), and four flow rates ($Q_{\text{tot}} = 0$, 20, 60, and 100 $\mu\text{L} / \text{min}$), PCL crystallinities were determined by XRD, as described previously; the results are presented in Figure 5 as plots of PCL crystallinity vs. flow rate for PCL-5k (A) and PCL-12k (B) NPs prepared in single-phase SHB (blue curves) and two-phase (red curves) reactors.

Figure 5A and Figure 5B show very similar trends for the PCL-5k and PCL-12k copolymers, respectively. Both copolymers self-assembled in the single-phase SHB reactor (blue) show PCL crystallinities that are independent of flow rate and are also similar to the bulk value (purple); these values for PCL-5k and PCL-12k are ~25% (50% of PCL crystallized) and ~40% (57% of PCL crystallized), respectively. In contrast, PCL crystallinities of both copolymers self-assembled in the two-phase reactor (red) increase linearly with flow rate, reaching values of ~45% for PCL-5k (90% of PCL crystallized) and ~68% for PCL-12k (97% of PCL crystallized) at $Q_{\text{tot}} = 100 \mu\text{L} / \text{min}$.

Similar to the morphologies and core dimensions discussed previously, PCL crystallinities as functions of flow rate in both reactors provide further evidence that shear effects— in this case shear-induced crystallization— that are operative in the two-phase reactor are not at play in the single-phase SHB reactor. The single-phase SHB reactor results further provide a “low-shear” baseline for the flow-dependent two-phase reactor results, allowing decoupling of on-chip mixing and shear effects on core crystallization. Finally, the results in Figure 5 show that, unlike the NP morphologies and dimensions discussed previously, PCL core crystallinity in the bulk (slow mixing/low shear case) is almost identical to values in the single-phase SHB mixer (fast mixing/low shear case). This result suggests that whereas mixing rate strongly affects the NP morphologies and dimensions, mixing rate has a much weaker effect on core crystallinities, which are mainly influenced by shear effects. We speculate that this difference is related to the slower time scale of PCL crystallite growth compared to that of micelle formation, such that differences in the times of dropwise water addition and fast, on-chip mixing have a much smaller impact on the former, slow process (crystallization) compared to the latter, fast process (micellization).

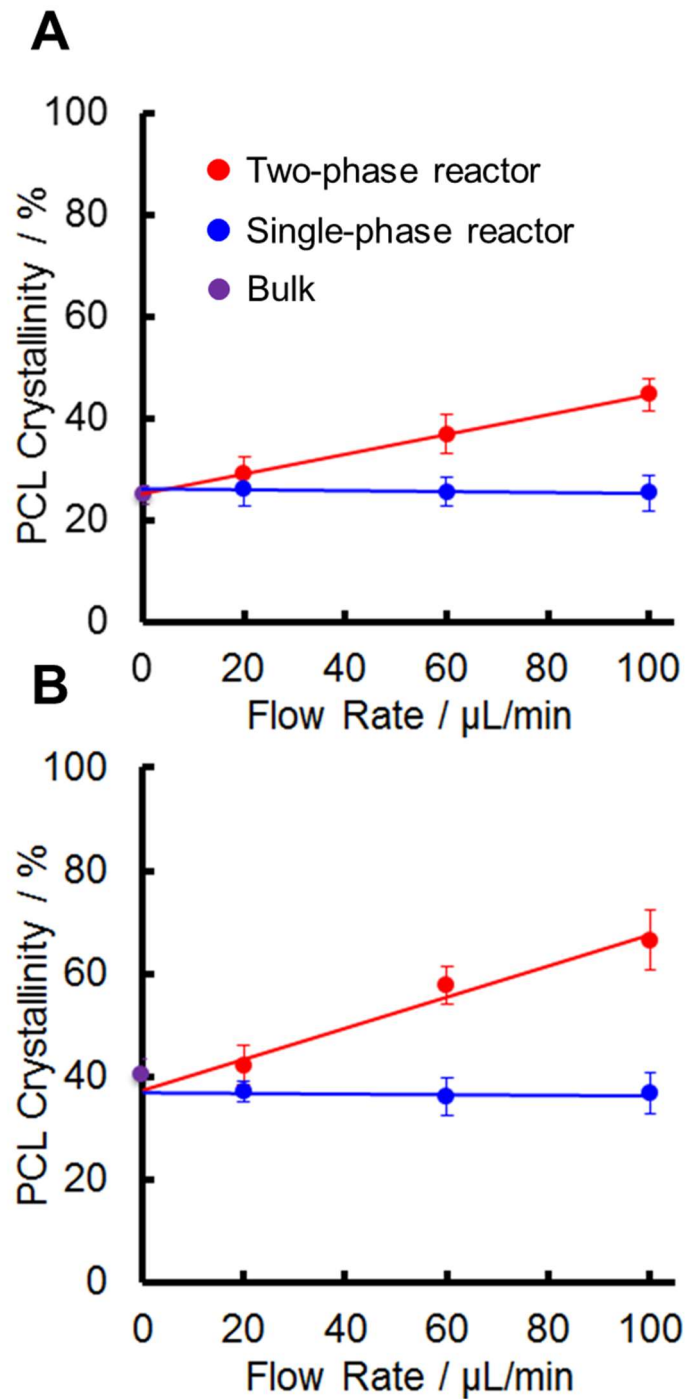


Figure 5. Effect of flow rate on mean PCL crystallinities of PCL-5k (A) and PCL-12k (B) NPs prepared in single-phase SHB (blue) and two-phase (red) microfluidic reactors and in the bulk (purple). Error bars are standard deviations from three separate preparations. Regression lines include fits to blue (single-phase SHB) and red (two-phase) data points, but are extended to the y-axis to show close agreement with the bulk (purple) data point.

Tuning Nanoparticle Multiscale Structure for Drug Delivery Applications.

Numerous studies highlight the importance of multiscale structure control for the application of polymeric nanoparticles to drug delivery. For example, on the colloidal scale (~10-100 nm), nanoparticle sizes and morphologies have been shown to strongly influence nanoparticle biodistributions and circulation times.⁵⁰⁻⁵² For intravenous carriers, colloidal particles less than 200 nm are believed to be resistant to uptake by phagocytic cells in the liver and spleen (RES clearance), whereas the kinetics and efficiency of uptake into targeted cells may also be size-dependent.⁵³ Another important size-dependent mechanism for delivery of anti-cancer agents is the enhanced permeability and retention (EPR) effect, in which particles larger than 40 kDa are passively localized within tumours due to abnormal and leaky vasculature in the cancerous tissue.⁵⁴ Morphological effects are less well-understood, although cylindrical micelles have been shown to have longer circulation times in rodents than spherical micelles, suggesting that specific delivery properties can be achieved *via* morphological control.⁵¹ Other studies have demonstrated that, in addition to size and shape, the internal nanoscale (~1-10 nm) structure of polymeric nanoparticles, including the ordering of semicrystalline hydrophobic chains, is germane to drug delivery function, affecting particle stabilities, flexibilities, and release rates.^{19,20,55,56}

Based on these considerations, microfluidic approaches to nanoparticle synthesis enabling continuous variability of structure and function on multiple length scales are highly desirable in the context of nanomedicine manufacturing. This comparative study shows that such variability can be achieved using total flow rate as an experimental control handle, but only in microfluidic reactors in which local shear rates are sufficiently high. Single-phase SHB reactors, although fast mixers with demonstrated capability for forming small, low-polydispersity

nanoparticles,^{22,28} do not offer the flow-variability of structure and function exhibited by two-phase gas-liquid segmented reactors. In separating microfluidic mixing and shear effects in this manner, this study opens the door to future reactor designs in which high shear, in addition to fast mixing, become the new figures of merit for controlled drug delivery formulations.

Conclusion

We compared single-phase SHB and two-phase microfluidic mixers with respect to the on-chip manufacturing of PCL-*b*-PEO NPs. NPs generated from two different copolymers with different PCL block lengths in both reactors and at three different flow rates were compared with respect to morphologies and dimensions determined by TEM and core crystallinities determined by XRD. The NP structures achieved using these microfluidic approaches were also compared to structures attained using the conventional dropwise water addition method in the bulk. Our work revealed three key findings: (i) NP morphologies and dimensions from the bulk preparation were different than those from either microfluidic mixer; however, NP crystallinities from the bulk and single-phase SHB mixer preparations were similar; (ii) NP morphologies, dimensions, and internal crystallinities from the single-phase SHB and two-phase mixers at the lowest flow rate were similar; and (iii) NPs morphologies, dimensions, and internal crystallinities changed with increasing flow rate in the two-phase mixer but not in the single-phase SHB mixer.

Flow-directed multiscale structure in polymeric colloids manufactured in gas-liquid two-phase reactors has been previously investigated as a convenient route to controlled function in drug delivery NPs. These results confirm the important role of high shear in two-phase microfluidic mixers for on-chip, flow-dependent particle processing, while decoupling the role of high shear (two-phase reactor only) from fast mixing (both single-phase SHB and two-phase reactors). Such insights into the relative roles of mixing and shear provide opportunities for new

microfluidic reactor designs further optimized for manufacturing polymeric colloids of low polydispersity and controlled structure and function.

Supporting Information. Data for cwc determination; table of actual flow conditions.

Acknowledgements. We are grateful to the Natural Sciences and Engineering Research Council of Canada, NSERC, for financial support, and to Precision Nanosystems, Inc. (PNI) for the loan of a prototype version of the NanoAssemblr™ microfluidic mixer. We also thank Dr. Shell Ip (PNI) for helpful discussions, and acknowledge Dr. Patrick Nahirney and the UVic EM lab (Department of Biology) for the continued use of their TEM.

References

- (1) Song, Y. J.; Modrow, H.; Henry, L. L.; Saw, C. K.; Doomes, E. E.; Palshin, V.; Holmes, J.; Kumar, C. S. S. R. Microfluidic synthesis of nanoparticles and their biosensing applications. *Chem Mater* **2006**, *18*, 2817-2827.
- (2) Elvira, K. S.; Solvas, X. C. I.; Wootton, R. C. R.; deMello, A. J. The past, present and potential for microfluidic reactor technology in chemical synthesis. *Nat Chem* **2013**, *5*, 905-915.
- (3) Lim, J. M.; Bertrand, N.; Valencia, P. M.; Rhee, M.; Langer, R.; Jon, S.; Farokhzad, O. C.; Karnik, R. Parallel microfluidic synthesis of size-tunable polymeric nanoparticles using 3D flow focusing towards *in vivo* study. *Nanomed-Nanotechnol* **2014**, *10*, 401-409.
- (4) Xu, S. Q.; Nie, Z. H.; Seo, M.; Lewis, P.; Kumacheva, E.; Stone, H. A.; Garstecki, P.; Weibel, D. B.; Gitlin, I.; Whitesides, G. M. Generation of monodisperse particles by using microfluidics: control over size, shape, and composition. *Angew Chem Int Ed* **2005**, *44*, 734-738.

- (5) Karnik, R.; Gu, F.; Basto, P.; Cannizzaro, C.; Dean, L.; Kyei-Manu, W.; Langer, R.; Forokhzad, O. C. Microfluidic platform for controlled synthesis of polymeric nanoparticles. *Nano Lett* **2008**, *8*, 2906-2912.
- (6) Anderson, D. G.; Xu, Q. B.; Hashimoto, M.; Dang, T. T.; Hoare, Y.; Kohane, D. S.; Whitesides, G. M.; Langer, R. Preparation of monodisperse biodegradable polymer microparticles using a microfluidic flow - focusing device for controlled drug delivery. *Small* **2009**, *5*, 1575-1581.
- (7) Brown, L.; McArthur, S. L.; Wright, P. C.; Lewis, A.; Battaglia, G. Polymersome production on a microfluidic platform using pH sensitive block copolymers. *Lab Chip* **2010**, *10*, 1922-1928.
- (8) Jahn, A.; Vreeland, W. N.; Gaitan, M.; Locascio, L. E. Controlled vesicle self-assembly in microfluidic channels with hydrodynamic focusing. *J Amer Chem Soc* **2004**, *126*, 2674-2675.
- (9) Steinbacher, J. L.; Moy, R. W. Y.; Price, K. E.; Cummings, M. A.; Roychowdhury, C.; Buffy, J. J.; Olbricht, W. L.; Haaf, M.; McQuade, D. T. Rapid self-assembly of core-shell organosilicon microcapsules within a microfluidic device. *J Amer Chem Soc* **2006**, *128*, 9442-9447.
- (10) Malmstadt, N.; Nash, M. A.; Purnell, R. F.; Schmidt, J. J. Automated formation of lipid-bilayer membranes in a microfluidic device. *Nano Lett* **2006**, *6*, 1961-1965.
- (11) Feng, Q.; Sun, J.; Jiang, X. Microfluidics-mediated assembly of functional nanoparticles for cancer-related pharmaceutical applications. *Nanoscale* **2016**, *8*, 12430-12443.
- (12) Lee, C.-Y.; Wang, W.-T.; Liu, C.-C.; Fu, L.-M. Passive mixers in microfluidic systems: a review. *Chem Eng J* **2016**, *288*, 146-160.

- (13) Kim, H.; Min, K.-I.; Inoue, K.; Kim, D.-P.; Yoshida, J.-i. Submillisecond organic synthesis: Outpacing Fries rearrangement through microfluidic rapid mixing. *Science* **2016**, *352*, 691-694.
- (14) Capretto, L.; Carugo, D.; Mazzitelli, S.; Nastruzzi, C.; Zhang, X. L. Microfluidic and lab-on-a-chip preparation routes for organic nanoparticles and vesicular systems for nanomedicine applications. *Adv Drug Deliver Rev* **2013**, *65*, 1496-1532.
- (15) Wang, C. W.; Sinton, D.; Moffitt, M. G. Flow-directed block copolymer micelle morphologies *via* microfluidic self-assembly. *J Am Chem Soc* **2011**, *133*, 18853-18864.
- (16) Wang, C. W.; Bains, A.; Sinton, D.; Moffitt, M. G. Flow-directed assembly of block copolymer vesicles in the lab-on-a-chip. *Langmuir* **2012**, *28*, 15756-15761.
- (17) Wang, C. W.; Bains, A.; Sinton, D.; Moffitt, M. G. Flow-directed loading of block copolymer micelles with hydrophobic probes in a gas-liquid microreactor. *Langmuir* **2013**, *29*, 8385-8394.
- (18) Xu, Z. Q.; Yan, B.; Riordon, J.; Zhao, Y.; Sinton, D.; Moffitt, M. G. Microfluidic synthesis of photoresponsive spool-like block copolymer nanoparticles: flow-directed formation and light-triggered dissociation. *Chem Mater* **2015**, *27*, 8094-8104.
- (19) Bains, A.; Cao, Y. M.; Moffitt, M. G. Multiscale control of hierarchical structure in crystalline block copolymer nanoparticles using microfluidics. *Macromol Rap Comm* **2015**, *36*, 2000-2005.
- (20) Bains, A.; Wulff, J. E.; Moffitt, M. G. Microfluidic synthesis of dye-loaded polycaprolactone-block-poly (ethylene oxide) nanoparticles: Insights into flow-directed loading and in vitro release for drug delivery. *J Coll Interf Sci* **2016**, *475*, 136-148.

- (21) Baek, S.; Song, S.; Lee, J.; Kim, J. M. Nanoscale diameter control of sensory polydiacetylene nanoparticles on microfluidic chip for enhanced fluorescence signal. *Sensor Actuat B-Chem* **2016**, *230*, 623-629.
- (22) Belliveau, N. M.; Huft, J.; Lin, P. J. C.; Chen, S.; Leung, A. K. K.; Leaver, T. J.; Wild, A. W.; Lee, J. B.; Taylor, R. J.; Tam, Y. K.; Hansen, C. L.; Cullis, P. R. Microfluidic synthesis of highly potent limit-size lipid nanoparticles for *in vivo* delivery of siRNA. *Mol Ther-Nucl Acids* **2012**, *1*.
- (23) Capretto, L.; Mazzitelli, S.; Brognara, E.; Lampronti, I.; Carugo, D.; Hill, M.; Zhang, X. L.; Gambari, R.; Nastruzzi, C. Mithramycin encapsulated in polymeric micelles by microfluidic technology as novel therapeutic protocol for beta-thalassemia. *Int J Nanomed* **2012**, *7*, 307-324.
- (24) Kastner, E.; Kaur, R.; Lowry, D.; Moghaddam, B.; Wilkinson, A.; Perrie, Y. High-throughput manufacturing of size-tuned liposomes by a new microfluidics method using enhanced statistical tools for characterization. *Int J Pharmaceut* **2014**, *477*, 361-368.
- (25) Krishna, K. S.; Li, Y. H.; Li, S. N.; Kumar, C. S. S. R. Lab-on-a-chip synthesis of inorganic nanomaterials and quantum dots for biomedical applications. *Adv Drug Deliver Rev* **2013**, *65*, 1470-1495.
- (26) Maeki, M.; Saito, T.; Sato, Y.; Yasui, T.; Kaji, N.; Ishida, A.; Tani, H.; Baba, Y.; Harashima, H.; Tokeshi, M. A strategy for synthesis of lipid nanoparticles using microfluidic devices with a mixer structure. *RSC Adv* **2015**, *5*, 46181-46185.
- (27) Mazzitelli, S.; Capretto, L.; Carugo, D.; Zhang, X. L.; Piva, R.; Nastruzzi, C. Optimised production of multifunctional microfibres by microfluidic chip technology for tissue engineering applications. *Lab Chip* **2011**, *11*, 1776-1785.

- (28) Zhigaltsev, I. V.; Belliveau, N.; Hafez, I.; Leung, A. K. K.; Huft, J.; Hansen, C.; Cullis, P. R. Bottom-up design and synthesis of limit size lipid nanoparticle systems with aqueous and triglyceride cores using millisecond microfluidic mixing. *Langmuir* **2012**, *28*, 3633-3640.
- (29) Schabas, G.; Wang, C. W.; Oskooei, A.; Yusuf, H.; Moffitt, M. G.; Sinton, D. Formation and shear-induced processing of quantum dot colloidal assemblies in a multiphase microfluidic chip. *Langmuir* **2008**, *24*, 10596-10603.
- (30) Wang, C. W.; Oskooei, A.; Sinton, D.; Moffitt, M. G. Controlled self-assembly of quantum dot-block copolymer colloids in multiphase microfluidic reactors. *Langmuir* **2010**, *26*, 716-723.
- (31) Johnson, T. J.; Ross, D.; Locascio, L. E. Rapid microfluidic mixing. *Anal Chem* **2002**, *74*, 45-51.
- (32) Knight, J. B.; Vishwanath, A.; Brody, J. P.; Austin, R. H. Hydrodynamic focusing on a silicon chip: Mixing nanoliters in microseconds. *Phys Rev Lett* **1998**, *80*, 3863-3866.
- (33) Stroock, A. D.; Dertinger, S. K. W.; Ajdari, A.; Mezic, I.; Stone, H. A.; Whitesides, G. M. Chaotic mixer for microchannels. *Science* **2002**, *295*, 647-651.
- (34) Stroock, A. D.; Dertinger, S. K.; Whitesides, G. M.; Ajdari, A. Patterning flows using grooved surfaces. *Anal Chem* **2002**, *74*, 5306-5312.
- (35) Howell, P. B.; Mott, D. R.; Fertig, S.; Kaplan, C. R.; Golden, J. P.; Oran, E. S.; Ligler, F. S. A microfluidic mixer with grooves placed on the top and bottom of the channel. *Lab Chip* **2005**, *5*, 524-530.
- (36) Lopez, M.; Graham, M. D. Enhancement of mixing and adsorption in microfluidic devices by shear-induced diffusion and topography-induced secondary flow. *Phys Fluids* **2008**, *20*, 053304.

- (37) Schwesinger, N.; Frank, T.; Wurmus, H. A modular microfluid system with an integrated micromixer. *J Micromech Microeng* **1996**, *6*, 99-102.
- (38) Song, H.; Tice, J. D.; Ismagilov, R. F. A microfluidic system for controlling reaction networks in time. *Angew Chem Int Edit* **2003**, *42*, 768-772.
- (39) Gunther, A.; Khan, S. A.; Thalmann, M.; Trachsel, F.; Jensen, K. F. Transport and reaction in microscale segmented gas-liquid flow. *Lab Chip* **2004**, *4*, 278-286.
- (40) Wang, C. W.; Sinton, D.; Moffitt, M. G. Morphological Control via Chemical and Shear Forces in Block Copolymer Self-Assembly in the Lab-on-Chip. *ACS Nano* **2013**, *7*, 1424-1436.
- (41) Lee, R.-S.; Hung, C.-B. Synthesis and characterization of amphiphilic block copolymers from poly (ethylene glycol) methyl ether and 4-methyl- ϵ -caprolactone or 4-phenyl- ϵ -caprolactone. *Polymer* **2007**, *48*, 2605-2612.
- (42) Wohlfarth, C.: Viscosity of the mixture (1) water; (2) *N,N*-dimethylformamide. In *Supplement to IV/18*; Lechner, M. D., Ed.; Springer Berlin Heidelberg: Berlin, Heidelberg, 2009; pp 757-760.
- (43) Williams, M. S.; Longmuir, K. J.; Yager, P. A practical guide to the staggered herringbone mixer. *Lab Chip* **2008**, *8*, 1121-1129.
- (44) Chen, G.; Hou, Y.; Knapp, H. Diffusion coefficients, kinematic viscosities, and refractive indices for heptane + ethylbenzene, sulfolane + 1-methylnaphthalene, water + *N,N*-dimethylformamide, water + methanol, water + *N*-formylmorpholine, and water + *N*-methylpyrrolidone. *J Chem Eng Data* **1995**, *40*, 1005-1010.
- (45) Hassell, D.; Zimmerman, W. Investigation of the convective motion through a staggered herringbone micromixer at low Reynolds number flow. *Chemical engineering science* **2006**, *61*, 2977-2985.

- (46) Son, Y. Determination of shear viscosity and shear rate from pressure drop and flow rate relationship in a rectangular channel. *Polymer* **2007**, *48*, 632-637.
- (47) Zhang, L.; Eisenberg, A. Multiple morphologies of "crew-cut" aggregates of polystyrene-*b*-poly(acrylic acid) block copolymers. *Science* **1995**, *268*, 1728-1731.
- (48) Zhang, L.; Eisenberg, A. Multiple morphologies and characteristics of "crew-cut" micelle-like aggregates of polystyrene-*b*-poly(acrylic acid) diblock copolymers in aqueous solutions. *J Am Chem Soc* **1996**, *118*, 3168-3181.
- (49) Rizis, G.; van de Ven, T. G. M.; Eisenberg, A. Crystallinity-driven morphological ripening processes for poly(ethylene oxide)-block-polycaprolactone micelles in water. *Soft Matter* **2014**, *10*, 2825-2835.
- (50) Cai, S.; Vijayan, K.; Cheng, D.; Lima, E. M.; Discher, D. E. Micelles of different morphologies—advantages of worm-like filomicelles of PEO-PCL in paclitaxel delivery. *Pharm. Res.* **2007**, *24*, 2099-2109.
- (51) Geng, Y.; Dalhaimer, P.; Cai, S.; Tsai, R.; Tewari, M.; Minko, T.; Discher, D. E. Shape effects of filaments versus spherical particles in flow and drug delivery. *Nat. Nanotech.* **2007**, *2*, 249-255.
- (52) Venkataraman, S.; Hedrick, J.; Ong, Z.; Yang, C.; Ee, P.; Hammond, P.; Yang, Y. The effects of polymeric nanostructure shape on drug delivery. *Adv Drug Deliver Rev* **2011**, *63*, 1228-1246.
- (53) Allen, C.; Maysinger, D.; Eisenberg, A. Nano-engineering block copolymer aggregates for drug delivery. *Coll. Surf. B* **1999**, *16*, 3-27.

- (54) Fang, J.; Nakamura, H.; Maeda, H. The EPR effect: unique features of tumor blood vessels for drug delivery, factors involved, and limitations and augmentation of the effect. *Adv Drug Deliver Rev* **2011**, *63*, 136-151.
- (55) Letchford, K.; Liggins, R.; Wasan, K.; Burt, H. *In vitro* human plasma distribution of nanoparticulate paclitaxel is dependent on the physicochemical properties of poly(ethylene glycol)-*block*-poly(caprolactone) nanoparticles. *Eur J Pharm Biopharm* **2009**, *71*, 196-206.
- (56) Glover, A. L.; Nikles, S. M.; Nikles, J. A.; Brazel, C. S.; Nikles, D. E. Polymer micelles with crystalline cores for thermally triggered release. *Langmuir* **2012**, *28*, 10653-10660.